



**HAL**  
open science

# Elephant modes and low frequency unsteadiness in a high Reynolds number, transonic afterbody wake

Philippe Meliga, D. Sipp, Jean-Marc Chomaz

► **To cite this version:**

Philippe Meliga, D. Sipp, Jean-Marc Chomaz. Elephant modes and low frequency unsteadiness in a high Reynolds number, transonic afterbody wake. *Physics of Fluids*, 2009, 21 (5), pp.054105. 10.1063/1.3139309 . hal-01021153

**HAL Id: hal-01021153**

**<https://polytechnique.hal.science/hal-01021153>**

Submitted on 15 Jul 2014

**HAL** is a multi-disciplinary open access archive for the deposit and dissemination of scientific research documents, whether they are published or not. The documents may come from teaching and research institutions in France or abroad, or from public or private research centers.

L'archive ouverte pluridisciplinaire **HAL**, est destinée au dépôt et à la diffusion de documents scientifiques de niveau recherche, publiés ou non, émanant des établissements d'enseignement et de recherche français ou étrangers, des laboratoires publics ou privés.



## Elephant modes and low frequency unsteadiness in a high Reynolds number, transonic afterbody wake

Philippe Meliga, Denis Sipp, and Jean-Marc Chomaz

Citation: *Physics of Fluids* (1994-present) **21**, 054105 (2009); doi: 10.1063/1.3139309

View online: <http://dx.doi.org/10.1063/1.3139309>

View Table of Contents: <http://scitation.aip.org/content/aip/journal/pof2/21/5?ver=pdfcov>

Published by the [AIP Publishing](#)

---

### Articles you may be interested in

[Low-frequency unsteadiness in the vortex formation region of a circular cylinder](#)

*Phys. Fluids* **25**, 085109 (2013); 10.1063/1.4818641

[Numerical simulation of subsonic and transonic turbulent flows in turbine cascades including wall heat flux and roughness](#)

*AIP Conf. Proc.* **1493**, 618 (2012); 10.1063/1.4765551

[Large eddy simulation of the flow around single and two side-by-side cylinders at subcritical Reynolds numbers](#)

*Phys. Fluids* **23**, 075101 (2011); 10.1063/1.3596267

[Aerodynamic loads on cactus-shaped cylinders at low Reynolds numbers](#)

*Phys. Fluids* **20**, 035112 (2008); 10.1063/1.2887982

[Stationary regimes of axisymmetric thermal wake interaction of two buoyant drops at low Reynolds and high Peclet number](#)

*Phys. Fluids* **18**, 072103 (2006); 10.1063/1.2219765

---

**AIP** | Journal of  
Applied Physics



*Journal of Applied Physics* is pleased to  
announce **André Anders** as its new Editor-in-Chief

# Elephant modes and low frequency unsteadiness in a high Reynolds number, transonic afterbody wake

Philippe Meliga,<sup>1,a)</sup> Denis Sipp,<sup>1</sup> and Jean-Marc Chomaz<sup>2</sup>

<sup>1</sup>ONERA/DAFE, 8 Rue des Vertugadins, 92190 Meudon, France

<sup>2</sup>LadHyX, CNRS-Ecole Polytechnique, 91128 Palaiseau, France

(Received 15 February 2009; accepted 7 April 2009; published online 20 May 2009)

Experiments and large eddy numerical simulation of a fully turbulent afterbody flow in the high subsonic regime, typical of that developing in the wake of a space launcher, exhibit a large-scale low frequency oscillation of the wake. In the present paper, we investigate to what extent the existence of the synchronized oscillations can be interpreted, at the high Reynolds numbers prevailing in this class of flows, by a local stability analysis of the mean flow, as measured in experiments or computed in numerical simulations. This analysis shows the presence of a pocket of absolute instability in the near wake, slightly detached from the body. The global frequency is strikingly well predicted by the absolute frequency at the upstream station of marginal absolute instability, this frequency selection being in agreement with the theory of nonlinear global modes. This result strongly suggests that a so-called elephant mode is responsible for the intense oscillations observed in the lee of space launcher configurations. © 2009 American Institute of Physics.

[DOI: 10.1063/1.3139309]

## I. INTRODUCTION

Experimental and numerical studies have shown that wake flows past axisymmetric bodies, such as spheres,<sup>1</sup> disks,<sup>2,3</sup> or axisymmetric blunt based bodies modeling an ideal rocket shape,<sup>4</sup> are dominated by an instability of helical modes of azimuthal wavenumbers  $m = \pm 1$ , resulting in the low frequency shedding of large-scale coherent structures. The use of local stability to analyze such self-sustained synchronized oscillations in free shear flows<sup>5</sup> at low Reynolds numbers suggests that they are linked to the existence of a region of local absolute instability in the near wake.<sup>6,7</sup>

Recent studies have considered the fully nonlinear regime associated with the existence of a pocket of absolute instability when the streamwise variations of the base flow are slow enough to apply the Wentzel–Kramers–Brillouin–Jeffreys (WKBJ) theory of slowly developing flows. Chomaz,<sup>8</sup> Couairon and Chomaz,<sup>9</sup> Tobias *et al.*,<sup>10</sup> Pier *et al.*,<sup>11</sup> analyzed the solutions of model equations in semi-infinite and infinite domains and discussed the connection between nonlinear global modes and front dynamics that characterize the propagation of a saturated instability wave into a quiescent region (see Ref. 12 for a review). If absolute instability arises beyond a specific downstream position  $z^{ca}$ , the nonlinear global mode, the so-called elephant mode, consists of a front pinned at the position  $z^{ca}$ . The front acts as the *wavemaker* and separates an upstream region where perturbations are evanescent, from a finite-amplitude wavetrain downstream. The global frequency is then given by the linear absolute frequency at the transition station  $z^{ca}$ , i.e.,  $\omega_G = \omega_r^0(z^{ca})$ , and the spatial growth rate at the front location is given by the absolute wavenumber  $-k_i^G = -k_i^0(z^{ca})$ . In the case of an absolutely unstable inlet condition, the same fre-

quency selection criterion remains valid only in the vicinity of the global instability threshold, whereas above the threshold, the front deforms to accommodate the inlet condition and the global frequency shifts from the absolute value.

Many of the results pertaining to the model equations have been shown to hold also in real flow situations, despite the fact that the slow streamwise variation assumption is not respected. In the case of the wake developing past a circular cylinder, the von Kármán vortex street presents a front located at  $z^{ca}$  and its frequency, as observed in direct numerical simulations, matches the absolute frequency  $\omega_r^0(z^{ca})$  within 10% accuracy over the range of Reynolds numbers  $100 \leq \text{Re} \leq 180$ .<sup>13</sup> Since then, several successful analyses have been carried out in the context of swirling jets,<sup>14</sup> hot round jets,<sup>15</sup> spiral vortex breakdown,<sup>16</sup> or interdisk flows,<sup>17</sup> but all these cases pertain to moderate Reynolds numbers. For large Reynolds numbers, Monkewitz<sup>18</sup> suggested that the low frequency oscillation of the wake of the sphere at Reynolds numbers  $\text{Re} = 6000$  was due to the absolute instability of the wake profile with sufficiently thin vorticity thickness. For such large Reynolds numbers, the key idea is that the leading convectively and absolutely unstable modes scale differently and explain different features of the flow. On the one hand, convective instability describes the spatially growing small-scale Kelvin–Helmholtz-like instability that develops in the separating shear layer and selectively amplifies the background noise and is responsible for the generation of turbulence in the wake. On the other hand, the absolute mode scales on the diameter of the wake. It grows slowly in space but is self-sustained in time. Because of this scale separation, these modes are believed to interact mainly through base flow modifications, the effect of the turbulent dissipation on the large-scale absolute mode being not presently addressed. A possible approach to address this question would be to substitute the constant molecular viscosity used in the laminar governing equations by a variable turbulent eddy viscos-

<sup>a)</sup>Present address: LadHyX, CNRS-Ecole Polytechnique. Electronic mail: philippe.meliga@ladhyx.polytechnique.fr.

ity modeling the interaction of the perturbations with the background turbulence. The latter turbulent viscosity can be deduced for instance from the mean velocity profiles issuing from a large eddy simulation (LES): Such an approach was proposed by del Álamo and Jiménez<sup>19</sup> to compute the linear amplification of energy in turbulent channel flows, but its extension to the present case deserves further investigation.

Recently, the stability analysis of compressible model wakes<sup>20</sup> with variable density has shown that the transition to absolute instability is led essentially by a low frequency, large-scale mode of azimuthal wavenumber  $m=1$ . These results have given credit to the interpretation of the large-scale oscillation observed in the wake of axisymmetric bodies in terms of a nonlinear global mode triggered by a local transition to absolute instability of this helical *wake* mode, since its azimuthal wavenumber and absolute frequency match the observations. However, agreement is only qualitative and can be fortuitous since at the transition point, the model profiles are far from representing the instantaneous or mean velocity profiles. Therefore, the aim of the present study is to analyze the stability of realistic velocity profiles, and so to investigate to what extent the dynamics of an afterbody flow, computed via a high resolution LES, in the fully turbulent and compressible regimes, may be interpreted using the local stability theory. In the context of such “industrial” applications, the steady axisymmetric base flow, i.e., the flow that would be naturally observed if all perturbations were damped, is not accessible and arclength continuation associated with Newton methods,<sup>21</sup> widely used at low Reynolds numbers to compute the base flow beyond the threshold of instability, cannot be pursued to such large Reynolds numbers. Only the mean flow, obtained by time and azimuth average, can be used to assess the stability properties, keeping in mind that this mean flow is not a solution of the steady axisymmetric Navier–Stokes equations.

## II. UNSTEADY DYNAMICS AND MEAN FLOW

The afterbody retained for this numerical study is taken from experiments carried out in ONERA’s S3Ch wind tunnel,<sup>22</sup> and was originally designed to model the first stage of a space launcher vehicle. The general configuration, shown in Fig. 1(a), is a cylindrical body of diameter  $D=100$  mm. The flow is subsonic, turbulent, of free-stream velocity  $W_\infty=235$  m/s, the total pressure and temperature being respectively of  $p_i=1.01 \times 10^5$  Pa and  $T_i=310$  K. The Mach and Reynolds numbers built from the diameter  $D$  and the free-stream quantities are 0.7 and  $1.2 \times 10^6$ , respectively. The wind tunnel configuration is detailed in the upper half of Fig. 1(b): A turbulent boundary layer develops on an upstream forebody of length 2.2 m. Its nondimensional thickness was measured to be  $\delta_{0.99}=0.2$  at the nondimensional upstream position  $z=-2.45$ , identified by the black circle in Fig. 1(b). Figure 2(a) shows the power spectral density (PSD) of wall pressure fluctuations  $G$ , measured experimentally 35 mm away from the axis [point labeled A in Fig. 1(a)], plotted as  $St G(St)$  in log/linear axes, where  $St$  is the Strouhal number defined as  $St=fD/W_\infty$  so that the energy contained in a peak is given by the area below that peak. In

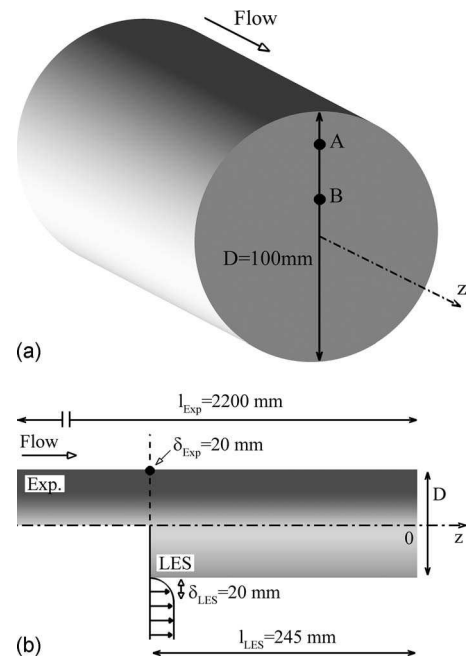


FIG. 1. Schematic of the axisymmetric afterbody model. (a) Three-dimensional view: The point labeled A is located 35 mm away from the revolution axis and corresponds to the experimental PSD shown in Fig. 2(a). The point labeled B is located 14 mm away from the revolution axis and corresponds to the numerical PSD shown in Fig. 2(b). (b) Side view: The upper half shows the experimental setup with the upstream forebody of length 2.2 m. The thickness of the turbulent boundary layer was measured 245 mm upstream from the base (black circle). The lower half shows the numerical modelization used for the LES.

the following, the notation  $St^*$  stands for Strouhal numbers measured from experimental and numerical data, whereas  $St$  denotes a value issuing from the local stability analysis. The spectrum is the average of 64 overlapping subtime intervals, the nondimensional frequency resolution being of 0.0085. In this fully turbulent regime, small scales are energetic and Fig. 2(a) shows a broad high frequency energy spectrum. We note the well defined energetic peak at  $St^*=0.20$ , corresponding to a low frequency oscillation. Similar results have also been reported in Ref. 23.

A LES of this configuration has been carried out using

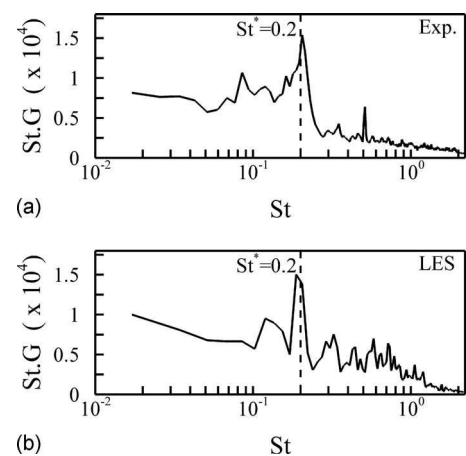


FIG. 2. PSD of the wall pressure fluctuations at the base. (a) Experimental measurements. (b) LES.

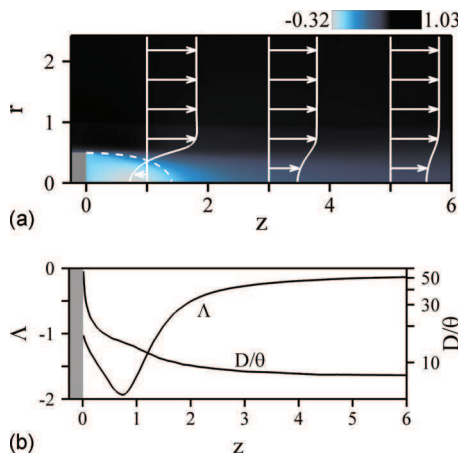


FIG. 3. (Color) LES mean flow obtained by time and azimuth average. (a) Axial velocity field. The dashed line stands for the edge of the recirculating bubble, marked by the streamline linking the separation point to the stagnation point on the axis. The axial velocity profiles  $\bar{W}(r)$  are superimposed for three streamwise locations ( $z=1, 3$ , and  $5$ ). (b) Streamwise evolution of the velocity ratio  $\Lambda(z)$  and of the steepness parameter  $D/\theta(z)$ .

the FLU3M code developed by ONERA, which solves the governing compressible Navier–Stokes equations on multi-block structured grids. Details, including time and space discretization and turbulence modeling, can be found in Ref. 24, where the agreement between numerical results and experimental data is assessed, validating the use of the LES solver. The retained configuration is shown in the upper half of Fig. 1: An inlet condition directly injects at the nondimensional upstream position  $z=-2.45$  a turbulent boundary layer around the cylinder shaped body, whose nondimensional thickness  $\delta=0.2$  corresponds to that measured in the experiments. Turbulence is forced by superimposing random fluctuations to this leading-order inlet condition. Removing the random fluctuations was found to have little influence on the numerical results. Figure 2(b) shows the PSD of the wall pressure fluctuations obtained from the numerical simulation, 14 mm away from the axis [point labeled  $B$  in Fig. 1(a)]. The total duration of the numerical simulation is about 20 ms, corresponding to about 10 low frequency cycles. The spectrum presented in Fig. 2 is obtained by averaging 15 overlapping samples, the frequency resolution being of 0.017. Although the numerical simulation gives access only to short time series, we obtain a good agreement between both spectra, in particular, we retrieve a well defined energetic peak at  $St^*=0.20$ , corresponding to the experimentally observed large-scale oscillation. Note that the high frequencies are more energetic in the LES calculation, this being probably due to the small difference in the location of the experimental and numerical measurements.

In the following, we use cylindrical coordinates  $(r, \theta, z)$  with origin taken at the center of the base.  $\rho$  is the density,  $p$  is the pressure,  $T$  is the temperature, and  $\mathbf{U}=(U, V, W)^T$  is the three-dimensional velocity field with  $U$ ,  $V$ , and  $W$  its radial, azimuthal, and streamwise components. The fluctuating non-axisymmetric three-dimensional field has been averaged in time and azimuth on the fly, during the calculation. The resulting mean flow  $\bar{\mathbf{Q}}=(\bar{\rho}, \bar{U}, \bar{V}=0, \bar{W}, \bar{T}, \bar{p})^T$  is therefore

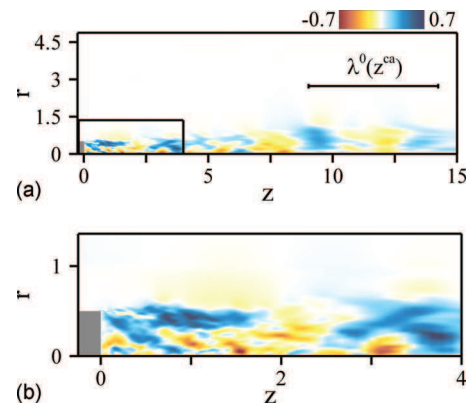


FIG. 4. (Color) (a) Instantaneous spatial structure of the  $m=1$  axial velocity coefficient  $\text{Re}(W_1)$  extracted from the LES calculations. (b) Close-up on the near wake area depicted in (a).

steady and axisymmetric. Figure 3(a) shows the mean axial velocity component: The classical topology of wake flows is retrieved, with a recirculation region of length  $\sim 1.33$  developing in the wake of the afterbody, and negative values of axial velocity reaching approximately 30% of the free-stream velocity. Figure 3(b) depicts the streamwise evolution of the velocity ratio  $\Lambda(z)=(\bar{W}_c(z)-\bar{W}_\infty)/(\bar{W}_c(z)+\bar{W}_\infty)$  and of the steepness parameter  $D/\theta(z)$ , where  $\theta$  is the momentum thickness defined as

$$\theta(z) = \int_0^\infty \frac{\bar{W}(r,z) - \bar{W}_c(z)}{\bar{W}_\infty - \bar{W}_c(z)} \frac{\bar{W}_\infty - \bar{W}(r,z)}{\bar{W}_\infty - \bar{W}_c(z)} dr, \quad (1)$$

where subscripts  $c$  and  $\infty$  refer to the centerline and to the free-stream quantities, respectively. The velocity ratio gets close to  $\Lambda=-2$  in the recirculating bubble, whereas the steepness parameter decays rapidly in the near wake and more slowly in the far wake, indicating that the shear layer thickens progressively as the flow develops. Note that the density ratio defined as  $S(z)=\bar{\rho}_c(z)/\bar{\rho}_\infty$  departs little from unity (not shown here).

An instantaneous velocity field  $\mathbf{U}(r, \theta, z)$  is decomposed into the azimuthal Fourier series

$$\mathbf{U}(r, \theta, z) = \sum_{m=-\infty}^{\infty} \mathbf{U}_m(r, z) e^{im\theta}. \quad (2)$$

The real part of the axial velocity coefficient  $\text{Re}(W_1)$  of the  $m=1$  component is presented in Fig. 4(a). The large-scale structure is visible downstream as an alternation of blue and red hues. Though, it is strongly modulated by a sea of small-scale turbulence close to the body, where the colored strips are blurred, as seen in Fig. 4(b).

### III. LOCAL STABILITY

The cross-stream and streamwise directions are both inhomogeneous directions for the mean flow, i.e.,  $\bar{\mathbf{Q}}(r, z)$ . At this point, we make the classical weakly nonparallel approximation, and consider the stability of the parallel flow, generated by neglecting the cross-stream velocity and extending to infinity the streamwise velocity profiles.<sup>25</sup> Disturbances

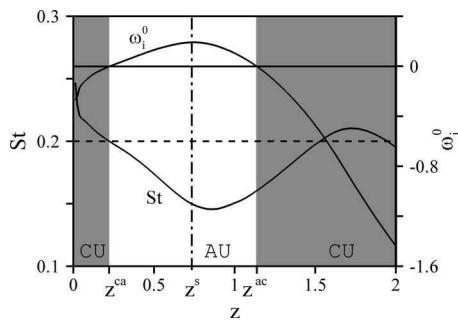


FIG. 5. Streamwise evolution of the Strouhal number  $St$  and of the absolute growth rate  $\omega_i^0$  obtained from the LES profiles. The solid horizontal lines represent the threshold of marginal absolute instability  $\omega_i^0=0$ . The dashed horizontal line marks the global frequency of the observed large-scale oscillations  $St^*=0.20$ . The shaded areas correspond to convectively unstable domains. The dashed-dotted line indicates the locus of the saddle point predicted by the linear global mode theory that turns out to be nearly real in the present case.

$\mathbf{q}' = (\rho', \mathbf{u}', p', t')^T$  to the parallel flow are chosen as normal modes  $\mathbf{q}'(r)e^{i(kz+m\theta-\omega t)}$  characterized by the complex axial wavenumber  $k = k_r + ik_i$ , the complex pulsation  $\omega = \omega_r + i\omega_i$ ,  $\omega_i$  and  $-k_i$  being the temporal and spatial growth rates, respectively, and the azimuthal wavenumber  $m$ . The local stability equations used to characterize the growth of such normal modes are identical to that detailed in Ref. 20. In particular, the viscosity of the fluid is considered constant, and no interaction of the disturbances with the background turbulence is considered here, as already mentioned for introductory purposes. For each streamwise station, the Reynolds and Mach numbers used in the perturbation equations are built from the mean velocity  $\bar{W}_m(z) = [\bar{W}_\infty + \bar{W}_c(z)]/2$ , the length scale  $l(z)$  defined as  $\bar{W}[l(z)] = \bar{W}_m(z)$  and the free-stream density and temperature. The Prandtl number remains constant and equal to unity.  $\mathbf{q}'$  is solution of the classical generalized eigenvalue problem for either  $k$  or  $\omega$ . This eigenvalue problem is solved using the Chebyshev collocation method discussed in Ref. 20. The local mean flow velocity, temperature, and density profiles, measured on the mesh of the LES simulation, are first interpolated on the collocation points of the stability solver using cubic spline interpolation. Complex pairs  $(k^0, \omega^0)$  corresponding to modes of zero group velocity (i.e.,  $\partial\omega/\partial k=0$ ) are then computed by the iterative technique described in Ref. 20. All results are ultimately rescaled and presented using the afterbody diameter and the free-stream velocity as reference scales. For all streamwise positions, we find that the transition to absolute instability is led by a large-scale  $m=1$  mode. This is consistent with the results presented in Ref. 20, in which the absolute instability has been shown to be led by the large-scale  $m=1$  wake mode for velocity ratios similar to that of the present LES velocity profiles. The streamwise variations of the Strouhal number based on the absolute frequency  $St = \omega_r^0/2\pi$  and that of the absolute temporal growth rate  $\omega_i^0$  are presented in Fig. 5. The solid and dashed horizontal lines stand for the threshold of marginal absolute instability  $\omega_i^0=0$  and for the global frequency of the observed large-scale oscillations  $St^*=0.20$ , respectively. The variations of the absolute wavelength  $\lambda^0 = 2\pi/k_r^0$  and of the absolute spatial growth rate  $-k_i^0$  are

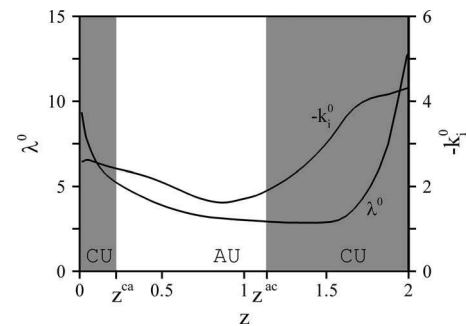


FIG. 6. Streamwise evolution of the absolute wavelength  $\lambda^0$  and of the absolute spatial growth rate  $-k_i^0$ . The shaded areas correspond to convectively unstable domains.

shown in Fig. 6. The mean flow is convectively unstable in an upstream region extending from the base to  $z^{ca}=0.23$ . Owing to the high rates of reverse flow at the centerline, absolute instability prevails in the domain  $z^{ca} < z < z^{ac}=1.14$ . Downstream of  $z^{ac}$ , the thickening of the shear layer and the decrease in magnitude of the counterflow induce a decrease in  $\omega_i^0$  to negative values, and thus the mean flow is convectively unstable. The observed global frequency  $St^*=0.20$  is predicted with excellent accuracy, by the absolute frequency  $\omega_r^0(z^{ca})=1.25$  corresponding to the same frequency  $St=0.20$  than that evidenced in the experimental and numerical spectra. The absolute wavelength and spatial growth rate at the transition station are  $\lambda^0(z^{ca})=5.21$  and  $k_i^0(z^{ca})=-2.41$ , respectively. The absolute wavelength  $\lambda^0(z^{ca})$  is shown in Fig. 4(a), and compares favorably with the spatial distribution of the large-scale  $m=1$  component. A more precise measure of the spatial wavelength associated to the  $St=0.20$  mode is presently not accessible since it would require the storage and processing of a time series of three-dimensional flow fields that would be far too glutton with the available computer resources. For the same reason, the spatial envelop of the  $St^*=0.2$  oscillation cannot be retrieved from the numerics and comparison of the front location and slope as in the studies of Gallaire *et al.* 16 or Lesshafft *et al.* 15 is not possible.

## IV. DISCUSSION

This study shows the existence of a pocket of absolute instability of the mean flow in the near wake of the afterbody, detached from the base. Although the large-scale contribution is partially overwhelmed by the small-scale turbulence at the high Reynolds number under consideration, the global frequency is well predicted by the absolute frequency at the upstream station of marginal absolute instability, which is located at the origin of the growing part of the  $m=1$  fluctuations. These results agree with the theory of nonlinear global modes, and make probable that a so-called elephant mode develops in the wake of the afterbody and is responsible for the large-scale synchronized oscillations.

In contrast, previous studies on the cylinder wake<sup>13,25,26</sup> have shown that up to the large Reynolds number  $Re=4600$ , the global frequency  $\omega_G$  is well predicted by the linear sta-

bility theory of slowly varying flows, also applied to the mean flow. In that case, the frequency  $\omega_G$  is given by the saddle point condition

$$\omega_G = \omega^0(z^s), \quad \frac{\partial \omega^0}{\partial z}(z^s) = 0. \quad (3)$$

Since derivatives of  $\omega^0(z)$  are known only along the real  $z$ -axis, the location of the saddle point  $z^s$  is found through the use of the Cauchy–Riemann equations and analytic continuation of  $\omega^0(z)$  in the complex  $z$ -plane.<sup>27</sup> Applying this linear global mode prediction to the present case, we obtain a saddle point at  $z^s = 0.735 - 0.022i$ , nearly on the real  $z$  axis, close to the position of the maximum absolute growth rate (see Fig. 5), associated with a Strouhal number  $St = 0.15$ , different from that found in the experimental and numerical spectra. We interpret this result in the following manner: in the weakly nonlinear approximation, Sipp and Lebedev<sup>28</sup> showed that in the case of the cylinder wake, resonance with the harmonics is weak, i.e., the leading-order nonlinear effects are restricted to base flow modifications. In this particular case, the mean flow is then approximately marginally stable and the global frequency predicted by the linear stability analysis of the mean flow approximates well the observed frequency, which explains the success of the saddle point condition (3). Though, this is not true anymore if resonance occurs with the harmonics of the global mode. In that more generic case, the linear stability analysis of the mean flow fails, i.e., the mean flow is no more marginally stable, and its frequency differs from the observed one. Figure 5 shows that the saddle point  $z^s$  is associated with a large growth rate  $\omega_i^0(z^s) = 0.19$ . This result indicates that the mean flow is presently strongly linearly unstable, and suggests that this configuration exhibits strong resonance with the harmonics of the global mode. The elephant mode theory, which predicts with amazing precision the observed frequency, does not suffer similar restrictions since harmonics forcing is at work in the saturated wave region downstream of the front so that departure from criticality can be arbitrary. It has been derived assuming only the flow to be weakly nonparallel, in order to use the WKBJ approximation.

The validity of this slowly varying approximation may be questioned, owing to the streamwise development of the mean flow. This can be done by considering the parameter  $\eta$  measuring the nonparallelism of the mean flow, defined as the ratio

$$\eta = \frac{1}{k_{\max}} \frac{1}{\theta} \frac{d\theta}{dz}, \quad (4)$$

where  $k_{\max}$  is the wavenumber of the most amplified temporal instability mode and  $\theta$  is the momentum thickness of the velocity profile  $\bar{W}(r, z)$  so that the ratio  $\theta^{-1} d\theta/dz$  characterizes the streamwise variations of the mean flow.<sup>25</sup> The streamwise evolution of  $\eta$  is shown in Fig. 7. Although  $\eta$  remains smaller than 5% for  $x > 2.5$ , we find that the nonparallel effects are quite important close to the stagnation points. As already observed in other configurations,<sup>15,17</sup> the elephant mode theory, which is solely an asymptotic theory in  $\eta$ , gives strikingly precise predictions of the frequency and spa-

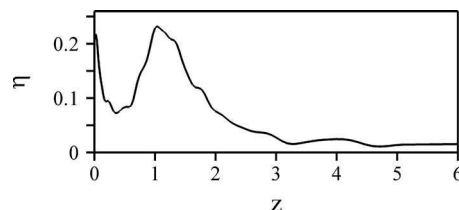


FIG. 7. Streamwise evolution of the parameter  $\eta$  measuring the nonparallelism of the spatially developing LES mean flow.

tial distribution of the nonlinear fluctuations, even in complex situations where high Reynolds numbers prevail, when it is outside its validity domain, in particular when the WKBJ approximation is not legitimate. It represents a guideline to understand the physical origin and eventually propose control strategies of the large-scale synchronized oscillations developing in the wake of realistic afterbodies.

Such a control may be achieved through base flow modifications, for instance, base bleed.<sup>4,29</sup> In this context, the implementation of optimization procedures would be considerably eased if predictions of the absolute frequency as a function of the streamwise position  $z$  could be obtained using the known stability properties of analytical profiles. Such an analysis is carried out in the Appendix, using the model wake profiles introduced by Monkewitz and Sohn.<sup>30</sup> We find that the associated predicted Strouhal number  $\tilde{St} = 0.22$  overestimates only by 10% that issuing from the experimental and numerical spectra. In this context of flow control, the use of fitted profiles hence provides with decent estimates of the global frequency that may be refined when needed by carrying out the stability analysis on the actual profiles.

## ACKNOWLEDGMENTS

This study was supported by the CNES (the French Space Agency) within the framework of the *Aerodynamics of Nozzles and Afterbodies* research and technology program. The authors are grateful to P. Reijasse for providing with the experimental data, and to E. Garnier for his help in the processing of the LES results.

## APPENDIX: FITTING OR NOT FITTING, ABOUT THE INFLUENCE OF THE MEAN FLOW PROFILES

Many experimental or numerical identification of absolutely unstable regions rely on the stability properties of analytical model profiles on which the actual mean flow measurements are systematically fitted.<sup>14,26</sup> The aim of the present appendix is to investigate, in the present case, to what extent such a fitting procedure alters the results of the stability analysis. For clarity, all results pertaining to the fitted profiles are noted with a  $\sim$  symbol. We have used the two-parameter  $(\tilde{A}, \tilde{N})$  model velocity profiles taken from Ref. 30, where the axial velocity profile reads

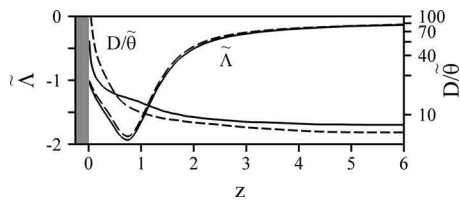


FIG. 8. Streamwise evolution of the fitted parameter  $\tilde{\Lambda}$  and of the fitted steepness parameter  $D/\tilde{\theta}$  (dashed lines). The values already shown in Fig. 3(b) are reported as solid lines for comparison.

$$\tilde{W}(r, z) = 1 + \frac{2\tilde{\Lambda}}{1 - \tilde{\Lambda}} F(r, z), \quad (\text{A1})$$

with

$$F(r, z) = \frac{1}{(2r^2 - 1)^{\tilde{N}(z)}}. \quad (\text{A2})$$

Since we consider here compressible flows, the temperature field is deduced from the fitted velocity profile through the Crocco–Busemann relation<sup>31</sup> and from the density ratio  $S = \bar{\rho}_c / \bar{\rho}_\infty$  computed at each streamwise station from the LES calculations. Finally, the density is obtained from the perfect gas state equation (see Ref. 20 for details).

For each streamwise position, the fitting parameters  $\tilde{\Lambda}(z)$  and  $\tilde{N}(z)$  have been determined using a standard least square method. The momentum thickness  $\tilde{\theta}$  of the fitted profile implicitly depends on  $\tilde{N}(z)$  as

$$\tilde{\theta}(z) = \int_0^\infty F(r, z) [1 - F(r, z)] dr. \quad (\text{A3})$$

Figure 8 depicts the streamwise evolution of  $\tilde{\Lambda}(z)$  and of the steepness parameter  $D/\tilde{\theta}(z)$  (dashed lines). The values of the LES parameters  $\Lambda(z)$  and  $D/\theta(z)$  introduced in Sec. II are also reported for comparison (solid lines). We observe a good agreement between the real and fitted velocity ratios, although the fitting procedure slightly underestimates the magnitude of the counterflow. However, the evolution of the shear parameter shows discrepancies, as the fitted momentum thickness of the developing wake overestimates (resp. slightly underestimates) that of the real profiles in the near wake (resp. in the far wake). Confirmation comes from Fig. 9 that shows a comparison between the LES profile and the corresponding fitted profile at the position  $z=0.05$ , within the recirculating bubble. We notice that the fitted profiles account neither for the small velocity overshoot existing just

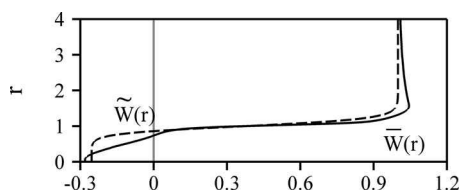


FIG. 9. Comparison between the LES (solid line) and the fitted (dashed line) velocity profiles at the streamwise station  $z=0.05$ .

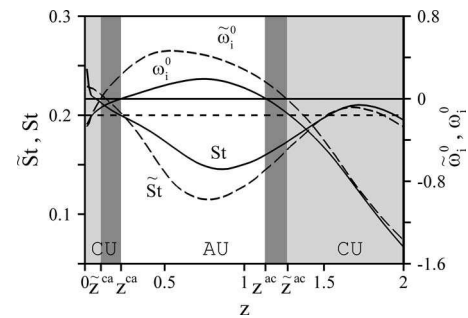


FIG. 10. Streamwise evolution of the Strouhal number  $\tilde{St}$  and of the absolute growth rate  $\tilde{\omega}_i^0$  obtained using fitted velocity profiles (dashed lines). The shaded areas correspond to convectively unstable domains. The solid lines refer to the results  $(St, \omega_i^0)$  presented in Fig. 5 for the real profiles. The solid horizontal line represents the threshold of marginal absolute instability  $\omega_i^0 = 0$ . The dashed horizontal line marks the global frequency of the observed large-scale oscillations  $St^* = 0.20$ .

outside of the shear-layer region, nor for the deformation of the velocity field close to the axis.

Figure 10 shows the streamwise variations of the Strouhal number based on the absolute frequency  $\tilde{St} = \tilde{\omega}_r^0 / 2\pi$  and that of the absolute growth rate  $\tilde{\omega}_i^0$  obtained using the fitted profiles (dashed lines). The solid lines refer to the Strouhal number  $St$  and to the absolute growth rate  $\omega_i^0$  shown in Fig. 5 for the exact LES profiles. The frequencies obtained from the fitted profiles match reasonably well with that obtained from the LES profiles. We find that absolute instability prevails in the domain  $\tilde{z}^{ca} = 0.01 < z < \tilde{z}^{ac} = 1.34$ , the amplification rates  $\tilde{\omega}_i^0$  being significantly overestimated in the whole absolute domain. As a result, using fitted profiles, the position of the upstream transition station that predicts the location of the front in the elephant mode theory, is slightly shifted upstream. In the range of parameters  $(\tilde{\Lambda}, D/\tilde{\theta}, S)$  prevailing in the near wake region, this can be explained by the fact that a higher steepness parameter results in a higher absolute growth rate  $\omega_i^0$ .<sup>20</sup> The global frequency selected at  $\tilde{z}^{ca}$ ,  $\tilde{\omega}_r^0(\tilde{z}^{ca}) = 1.39$ , corresponds to a Strouhal number of  $\tilde{St} = 0.22$  that moderately overestimates the global frequency obtained for the real profiles by 10%. Thus, the results obtained by fitting the actual LES profiles by model analytical profiles (A1) and (A2) agree reasonably well with the experimental observations and with the results issuing from the stability analysis of the exact LES profiles. In this specific case, this result therefore demonstrates the validity of the use of model profiles to estimate the global frequency with limited discrepancy.

<sup>1</sup>E. Achenbach, “Vortex shedding from spheres,” *J. Fluid Mech.* **62**, 209 (1974).

<sup>2</sup>H. V. Fuchs, E. Mercker, and U. Michel, “Large-scale coherent structures in the wake of axisymmetric bodies,” *J. Fluid Mech.* **93**, 185 (1979).

<sup>3</sup>E. Berger, D. Scholz, and M. Schumm, “Coherent vortex structures in the wake of a sphere and a circular disk at rest and under forced vibrations,” *J. Fluids Struct.* **4**, 231 (1990).

<sup>4</sup>A. Sevilla and C. Martínez-Bazán, “Vortex shedding in high Reynolds number axisymmetric bluff-body wakes: Local linear instability and global bleed control,” *Phys. Fluids* **16**, 3460 (2004).

<sup>5</sup>P. A. Monkewitz and L. N. Nguyen, “Absolute instability in the near-wake of two-dimensional bluff-bodies,” *J. Fluids Struct.* **1**, 165 (1987).

- <sup>6</sup>R. J. Briggs, *Electron Stream Interaction With Plasmas* (MIT, Cambridge, 1964).
- <sup>7</sup>A. Bers, "Linear waves and instabilities," in *Plasma Physics*, edited by C. De Witt and J. Peyraud (Gordon and Breach, New York, 1975), pp. 117–215.
- <sup>8</sup>J.-M. Chomaz, "Absolute and convective instability in non linear systems," *Phys. Rev. Lett.* **69**, 1931 (1992).
- <sup>9</sup>A. Couairon and J.-M. Chomaz, "Absolute and convective instabilities, front velocities and global modes in nonlinear systems," *Physica D* **108**, 236 (1997).
- <sup>10</sup>S. M. Tobias, M. R. E. Proctor, and E. Knobloch, "Convective and absolute instabilities of fluid flows in finite geometry," *Physica D* **113**, 43 (1998).
- <sup>11</sup>B. Pier, P. Huerre, and J.-M. Chomaz, "Bifurcation to fully nonlinear synchronized structures in slowly varying media," *Physica D* **148**, 49 (2001).
- <sup>12</sup>J.-M. Chomaz, "Global instabilities in spatially developing flows: Non-normality and nonlinearity," *Annu. Rev. Fluid Mech.* **37**, 357 (2005).
- <sup>13</sup>B. Pier, "On the frequency selection of finite-amplitude vortex shedding in the cylinder wake," *J. Fluid Mech.* **458**, 407 (2002).
- <sup>14</sup>F. Gallaire and J.-M. Chomaz, "Mode selection in swirling jet experiments: a linear stability analysis," *J. Fluid Mech.* **494**, 223 (2003).
- <sup>15</sup>L. Lesshafft, P. Huerre, P. Sagaut, and M. Terracol, "Nonlinear global modes in hot jets," *J. Fluid Mech.* **554**, 393 (2006).
- <sup>16</sup>F. Gallaire, M. Ruith, E. Meiburg, J.-M. Chomaz, and P. Huerre, "Spiral vortex breakdown as a global mode," *J. Fluid Mech.* **549**, 71 (2006).
- <sup>17</sup>B. Viaud, E. Serre, and J.-M. Chomaz, "The elephant mode between two rotating disks," *J. Fluid Mech.* **598**, 451 (2008).
- <sup>18</sup>P. A. Monkewitz, "A note on vortex shedding from axisymmetric bluff bodies," *J. Fluid Mech.* **192**, 561 (1988).
- <sup>19</sup>J. C. del Álamo and J. Jiménez, "Linear energy amplification in turbulent channels," *J. Fluid Mech.* **559**, 205 (2006).
- <sup>20</sup>P. Meliga, D. Sipp, and J.-M. Chomaz, "Absolute instability in axisymmetric wakes: compressible and density variation effects," *J. Fluid Mech.* **600**, 373 (2008).
- <sup>21</sup>D. Barkley, M. G. M. Gomes, and R. D. Henderson, "Three-dimensional instability in flow over a backward-facing step," *J. Fluid Mech.* **473**, 167 (2002).
- <sup>22</sup>D. Deprés, P. Reijasse, and J.-P. Dussauge, "Analysis of unsteadiness in afterbody transonic flows," *AIAA J.* **42**, 2541 (2004).
- <sup>23</sup>J.-P. Flodrops and J.-M. Dese, "Sillage d'un culot axisymétrique," Institut de Mécanique des Fluides de Lill Report No. 85/19, 1985.
- <sup>24</sup>S. Deck, E. Garnier, and P. Guillen, "Turbulence modelling applied to space launcher configurations," *J. Turbul.* **3**, 1 (2002).
- <sup>25</sup>D. Hammond and L. Redekopp, "Global dynamics of symmetric and asymmetric wakes," *J. Fluid Mech.* **331**, 231 (1997).
- <sup>26</sup>M. Khor, J. Sheridan, M. C. Thompson, and K. Hourigan, "Global frequency selection in the observed time-mean wakes of circular cylinders," *J. Fluid Mech.* **601**, 425 (2008).
- <sup>27</sup>P. Huerre and P. A. Monkewitz, "Absolute and convective instabilities in free shear layers," *J. Fluid Mech.* **159**, 151 (1985).
- <sup>28</sup>D. Sipp and A. Lebedev, "Global stability of base and mean flows: A general approach and its applications to cylinder and open cavity flows," *J. Fluid Mech.* **593**, 333 (2007).
- <sup>29</sup>A. Sevilla and C. Martínez-Bazàn, "A note on the stabilization of bluff-body wakes by low density base bleed," *Phys. Fluids* **18**, 098102 (2006).
- <sup>30</sup>P. A. Monkewitz and K. D. Sohn, "Absolute instability in hot jets," *AIAA J.* **26**, 911 (1988).
- <sup>31</sup>H. Schlichting, *Boundary Layer Theory*, 7th ed. (McGraw-Hill, New York, 1978).